We are IntechOpen, the world's leading publisher of Open Access books Built by scientists, for scientists

6,900
Open access books available

185,000
International authors and editors

200M
Downloads

Our authors are among the

154
Countries delivered to

TOP 1%
most cited scientists

12.2%
Contributors from top 500 universities



WEB OF SCIENCE™

Selection of our books indexed in the Book Citation Index in Web of Science™ Core Collection (BKCI)

Interested in publishing with us?
Contact book.department@intechopen.com

Numbers displayed above are based on latest data collected.
For more information visit www.intechopen.com



38

Mechanical Alloying: For Formation of Nanocomposite WC/MgO Materials

Shigen Zhu, Jun Ma, Meilin Zhang and Caixia Wu
Donghua University
P.R.China

1. Introduction

Composites are the combination of two or more materials in which tailored properties are achieved by bringing the combined advantages of both reinforcement and matrix into full play, which gives us a rather high degree of freedom in material design (Zhang et al., 1997). Structurally, reinforcements may be in the form of fibers, particles or whiskers, and recent interest has been attracted on the nanostructured composites (Kalambur & Hall, 1997). Because of the extremely small size of the grains, a large fraction of the atoms in these materials is located in the grain boundaries and thus the composites exhibits enhanced combinations of physical, mechanical and magnetic properties (Koch, 1993; Suryanarayana, 1995; Gleiter, 1989; Suryanarayana & Koch, 1999). Nanocomposites illustrate increased strength, high hardness, extremely high diffusion rates, and consequently reduced sintering times for powder compaction.

Some composites, like WC-Co, have shown an exceptional high value of hardness, and good wear/corrosion resistance. It has been widely used for machining, cutting, wearing, as well as high performance construction and apparatus. However, the process to produce WC-Co is very complicated and costly in the reason that the main component WC is usually obtained by direct synthesis of elemental W and C at high temperature and Co is rare and expensive. Many efforts have been focused on reducing the fabrication cost and finding new materials as the alternative for Co. Fortunately, we have employed a high-energy planetary ball mill to prepare a composite of WC toughened with MgO. The results illustrated that the nanocomposite WC/MgO offered unique combination of high hardness and excellent fracture toughness, which is comparable to the properties of WC-Co. Furthermore, the high-energy planetary ball mill, one kind of mechanical alloying (MA), has been a one-step successful route in synthesizing this compound in powder forms in an inexpensive and faster way.

Mechanical alloying (MA) is a solid-state powder processing techniques involving repeated welding, fracturing and rewelding of powder particles in a high-energy ball mill. MA has now been shown to be capable of synthesizing a variety of equilibrium and non-equilibrium alloy phases starting from blended elemental or prealloyed powders (Benjanmin, 1970; Wright & Wilcox, 1974; Gessinger, 1976; Koch et al, 1983; Schwarz & Koch, 1986; Sherif El-Eskandarany, 1996; Sherif El-Eskandarany et al., 1997). During the past few years, considerable of equilibrium and metastable alloy phases have been synthesized by this simple and inexpensive processing technique – mechanical alloying/milling of metal

powders, including oxide dispersion strengthened materials, supersaturated solid solutions, non-equilibrium crystalline or quasicrystalline intermediate phases and amorphous alloys (Doppiu et al., 2007; Razavi et al., 2008; Legendre et al., 2007).

The present chapter will be a guided introduction to the fabrication of nanocomposites WC/MgO using MA method. The outline of the chapter will be as follows. In Section 2 of this chapter, we will briefly discuss the formation of nanocomposite WC/MgO powders and the mechanism of mechanical alloying at first. This will be followed by a description of the process and process variables. Recent developments in understanding the process of MA through modelling and milling maps are briefly described in Section 2.2, and then the application of artificial neural network (ANN) modelling method in MA process is described. The unique problem of process control agent (PCA) is discussed in Section 2.4. The last Section will present the consolidation of nanocomposite WC/MgO powders.

2. Formation of nanocomposite WC/MgO powders by high-energy planetary ball milling method

Refractory compounds, like WC, are usually synthesized on a commercial scale by direct reduction of metal with the appropriate reactants at high temperatures and pressures. The process is cumbersome, time-consuming and expansive, and the end product is heterogeneous. Mechanical alloying (MA) can be an ideal one-step successful route in synthesizing these compounds. Following is a guided introduction to the details involved in the fabrication of nanocomposite WC/MgO powders *via* MA method.

2.1 Formation of nanocomposite WC/MgO powders and its mechanisms

Reactant mixture powders are commercial powders of WO_3 (1.3 μm, 99.9 %), graphite (1 μm, 99.9 %) and Mg (50 μm, 99.5 %). These powders are mixed at an atomic ratio of 1:1:3. The ball milling experiments are carried out using a QM-1SP4 planetary ball milling machine under argon gas atmosphere. Details of the milling conditions are described in (Zhang et al., 2010). The weight of the powder mixture put into the milling vial is 20g.

The XRD patterns of the mixed powders after milling for different time is showed in Fig. 1. It indicated that the powder milled was a mixture of polycrystalline WO_3, graphite and Mg powders at the initial stage of milling. During high-energy ball milling, the powder particles are repeatedly flattened, cold welded, fractured and rewelded. In this early stages of milling, many new surfaces are created, and they enable the particles to weld together leading to an increase in particle size. Meanwhile, heavy deformation is introduced into the particles. This is manifested by the presence of a variety of crystal defects including dislocations, vacancies, stacking faults, and increased number of grain boundaries. These defect structures enhance the diffusivity of solute elements into the matrix. The composite particles at this stage have a layer structure consisting of various combinations of the starting components (Suryanarayana, 2001).

With further deformation, the particles get work hardened and fractured by a fatigue failure mechanism and/or by the fragmentation of fragile flakes (Suryanarayana, 2004). At this state, the fragments may predominate in reducing the particle size, and the strong agglomerating forces induced by cold welding may be absent. The refined microstructure feature decrease the diffusion distances. Additionally, the slight increase in temperature during milling further helps the diffusion behaviour.

After milling 4.7 h, the diffraction peaks coming from initial elemental powders were no longer visible, and the new diffraction peaks corresponding to WC and MgO phases were detected. When the powder was further milled, the feature of the milled powders XRD patterns did not change. It indicated that a reaction was ignited and finished completely within 4.7 h, leading to the formation of WC and MgO. Thus, the occurrence of the reaction during the ball milling was not gradual but abrupt in a very short milling time. Furthermore, it can be seen that the diffraction peaks were evidently broadened with the increasing of milling time, proving that the milling caused refinement of the particles grains. Consequently, nano-sized WC/MgO powders were obtained after milling for 50 h. This steady-state equilibrium is attained when a balance is achieved between the rate of welding, which increases the particle size, and the rate of fracturing, which decreases the composite particle size.

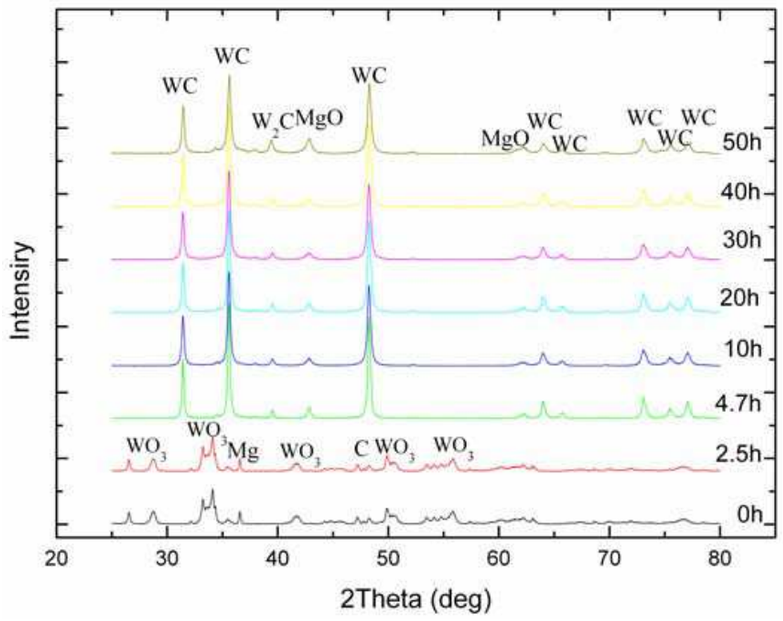


Fig. 1. The XRD patterns of the mixed powders after milling for different time

From above experimental results, it can be concluded that the oxidation-reduction reaction occurred among WO_3, graphite and Mg by high-energy milling and WC/MgO were formed. The reaction can be supposed as follows:

$$WO_3 + 3Mg \rightarrow W + 3MgO \tag{1}$$

$$W + C \rightarrow WC \tag{2}$$

where the metal oxide (WO_3) is reduced by a more reactive metal (Mg) to the pure metal (W). The reaction (1) is characterized by a large negative free energy (ΔG=-320kJ) and are therefore thermodynamically feasible at room temperature. The occurrence of the reaction at ambient temperatures is thus limited by kinetic consideration alone.

MA can provide the means to substantially increase the reaction kinetics of the reduction reactions. This is due to the repeated welding and fracturing of powder particles increases

the area of contact between the reactant powder particles which causes a reduction in particle size and allows fresh surfaces to come into contact repeatedly; this allows the reaction to proceed without the necessity for diffusion through the product layer. As a consequence, reactions that normally require high temperatures will occur at lower temperatures during MA without any externally applied heat. In addition, the high defect densities induced by MA accelerate the diffusion process. Alternatively, the particle refinement and consequent reduction in diffusion distances (due to microstructural refinement) can at least reduce the reaction temperatures significantly, even if they do not occur at room temperature.

The high temperature caused by the reaction (1) in the vial expedites the subsequent diffusion reaction of high activity W and C (reaction (2)). The reaction (2) is completed in a very short time. It can be seen from Fig. 1 that all W diffraction peaks disappeared, which is attributed to the diffusion reaction of C particles with W particles in high chemical activity.

In a word, the formation of such composite WC/MgO powders is attributed to the impact energy by high energy ball milling. Due to the impact energy, the superficial activity of Mg and the temperature of local areas increased, which enhanced the reaction between WO_3 and the Mg surface. When this reaction occurs, lots of heat released is enough to form WC between the W and C. From above analysis, it can be concluded that the mechanically induced self-sustained reaction can take place among a mixture of elemental WO_3, graphite and Mg according to reaction (1) and (2) during ball milling and completed in a very short time.

2.2 Modeling studies and milling maps

Generally, the reaction induced by high-energy ball milling can be a self-propagation high-temperature synthesis reaction (SHS) or a gradual diffusion reaction depending on the milling conditions. Different reaction kinetics are attributed to several factors, including thermodynamics, atomic and thermal diffusivity and the mechanical properties of the reactant powders, especially the processing factors such as milling speed, ball-to-powder weight ratio and milling ball diameter. These processing factors will determine the rate of energy transference from milling balls to the powder particles of the processed material. Suryanarayana et al. pointed out that if the energy transferred to powders is rather low, gradual reaction can be the reaction mode, while if it is sufficient high, SHS can be initiated (Suryanarayana et al., 2001).

According to recent studies (Magini & Iasonna, 1995; Magini et al., 1996; Murty et al., 1995; Rojac et al., 2006; Yang et al., 1997), milling maps can be an adaptive method to correlate the milling parameters with the ball milling energy transfer, as well as with the reaction mode. Burgio et al. (Burgio et al., 1991) have derived a set of kinematic equations to estimate the ball-to-powder energy transfer occurring in a single collision event. Magini et al. (Magini et al., 1996) have further studied the collision model, using the energy transfer per impact and the degree of filling for milling maps to the Pd-Si, Fe-Zr and Ti-Al system. Murty et al. (Murty et al., 1995) also have given the milling maps of $Ti_{50}Ni_{50}$ and $Ti_{50}Cu_{50}$ materials, and Rojac et al. (Rojac et al., 2006) have used ball impact energy and cumulative kinetic energy to develop a milling map for $NaNbO_3$.

Herein, the formation mode of WC/MgO is discussed. The experimental details are described in (Wu et al., 2009). The milling conditions adopted in the study is summarized in Table 1.

Milling speed (rpm)	100 150 200
Ball-powder weight ratio	5:1 10:1 15:1 20:1
Number of milling balls	15 30 45 60
Diameter of milling balls (mm)	10
Weight of each milling ball (g)	6.67
Volume of milling vial (ml)	250
Milling ball/ vial medium	Refractory alloy
Density of milling ball/vial (kg/m^3)	15×10^3

Table 1. The milling conditions adopted in the present study

Fig. 2 shows that the formation mode and the time required for the formation of WC/MgO varied depending on the milling conditions. WC/MgO powders can be synthesized either by SHS or by gradual reaction, and the time required for the formation of WC/MgO (determined from the XRD patterns) in general decreases with the increase in milling speed and ball-to-powder weight ratio.

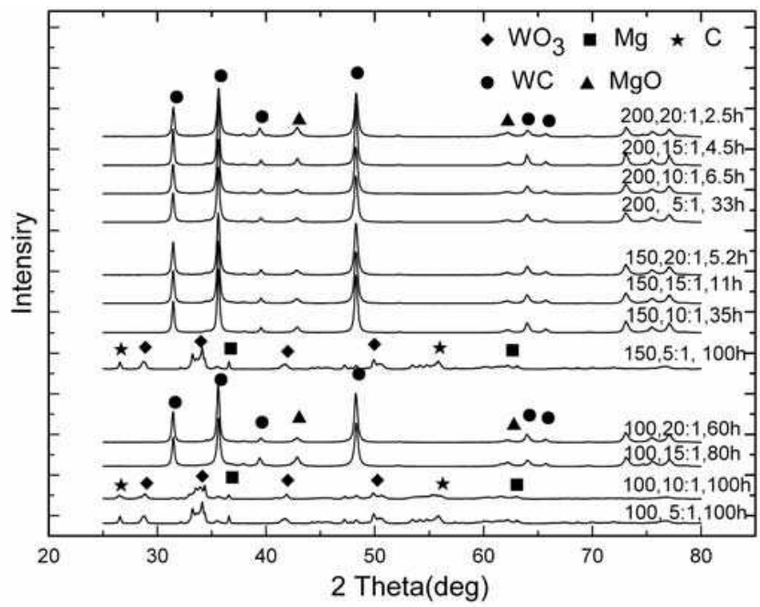


Fig. 2. XRD patterns of powders milled at different milling speed and ball-to-powder weight ratio for different milling time

All these results can be better understood when considering the energy transfer during milling. Magini et al., Murty et al. and Yang et al. have made some earlier efforts on the proposal of respective milling models (Magini et al., 1996; Murty et al., 1995; Yang et al., 1997). On the basis of these widely used milling models, the energy for the formation of WC/MgO by high-energy ball milling is analyzed, and details are described as follows:
The average linear velocity (V_b) and free distance (S) of the milling ball are given by (Yang et al., 1997)

$$V_b = 0.5 \cdot \omega_p \cdot r_0 \tag{3}$$

$$S = 2.228 \cdot r_b \cdot \sqrt[3]{\frac{\rho_b \cdot V_G}{R_{bp} \cdot m_p}} \tag{4}$$

where ω_p is the milling speed of disc, r_0 the radius of the vial, r_b the radius of the milling ball, ρ_b the density of ball, V_G the volume of the vial , R_{bp} the ball-to-powder weight ratio, and m_p the mass of the powder canned in the vial. Then, the collision frequency of each ball can be obtained through the following equation:

$$\nu = \frac{V_b}{S} \tag{5}$$

The energy transferred per unit of mass can be expressed by (Magini et al., 1996):

$$\frac{\Delta E}{Q_{\max}} = 7.66 \times 10^{-2} \cdot R_p^{1.2} \cdot \rho_b^{0.6} \cdot E^{0.4} \cdot \omega_p^{1.2} \cdot d_b / \sigma \tag{6}$$

where Q_{max} is the maximum quantity of trapped material, R_p the distance between center of disk and center of vial (R_p=0.115 m), ρ_b, E and d_b is the density, Young modulus and diameter of the milling balls respectively, and σ is the surface density of the covering powder. For refractory ball, ρ_b is 15×10^3 kg/m^3 and E is 5.5×10^{11} N/m^2. By measuring the weight of balls with several interruptions during the milling, σ is estimated to be about 0.25 mg/mm^2. Please note that the energy is absorbed only by a small quantity of mass trapped in a collision but not by the total powders. We should take all the milling balls into account when considering the influence of ball-to-powder weight ratio. Consequently, the total energy transferred per unit of mass and time can be described by

$$E_b^* = \phi_b \cdot \Delta E \cdot \nu \cdot n_b \tag{7}$$

where n_b is the number of milling balls, ϕ_b is an efficiency factor related to the filling of the vial, which is close to 1 for 1/3 filling of the vial (Magini et al., 1996) and the filling level in the present work is lower than 1/3. Thus Eq. (7) can be rewritten by

$$E_b = \Delta E \cdot \nu \cdot n_b \tag{8}$$

E_b is the effective extensive factor. On the hypothesis that all the milling energy is transferred to the powders, the energy accumulation with the increase of milling time (t), the milling time request for synthesizing WC/MgO) should be considered, thereby the total energy can be expressed by (Murty et al., 1995)

$$E_t = \frac{E_b \cdot n_b \cdot \nu \cdot t}{m_p} \tag{9}$$

The above parameters for different milling conditions are calculated and listed in Table 2. To verify Eq. (8), a number of experiments on the WO_3-C-3Mg system have been carried out at various milling speed and ball-to-powder weight ratio. Fig. 3 shows the change of the milling parameters with the different reaction modes. The SHS reaction might occur when the effective intensive factor E_b is over 38.24 kJ·g^{-1}·s^{-1}. The WC/MgO can be obtained through the gradual reaction when the E_b is 22.12~38.24 kJ·g^{-1}·s^{-1}. No WC/MgO can be

formed when the value of E_b is below 22.12 kJ·g^{-1}·s^{-1}. The milling energy maps would be of the prediction for other experiments carried out on the WO_3-C-3Mg system in the different milling conditions.

Milling speed ω_p (rpm)	Ball-powder weight ratio R_{bp}	Linear velocity V_b (m·s^{-1})	Collision frequency v (s^{-1})	Energy transferred per unit of mass ΔE (J/g·hit)	Effective extensive factor E_b (kJ·g^{-1}·s^{-1})	Milling Time t (h)	Total energy $E_t/10^6$ (kJ·g^{-1})
100	5:1	0.21	5.55	51.80	4.31		
	10:1		8.81		13.69		
	15:1		9.49		22.12	80	141.58
	20:1		10.08		31.34	60	112.83
150	5:1	0.31	8.32	84.26	10.52		
	10:1		15.13		38.24	35	160.61
	15:1		15.92		60.38	11	53.14
	20:1		16.65		84.18	5.2	26.26
200	5:1	0.42	11.13	119.00	19.81	33	156.91
	10:1		22.24		79.25	6.5	61.82
	15:1		23.09		123.64	4.5	44.51
	20:1		23.91		170.75	2.5	25.61

Table 2. Related parameters calculated at different milling conditions

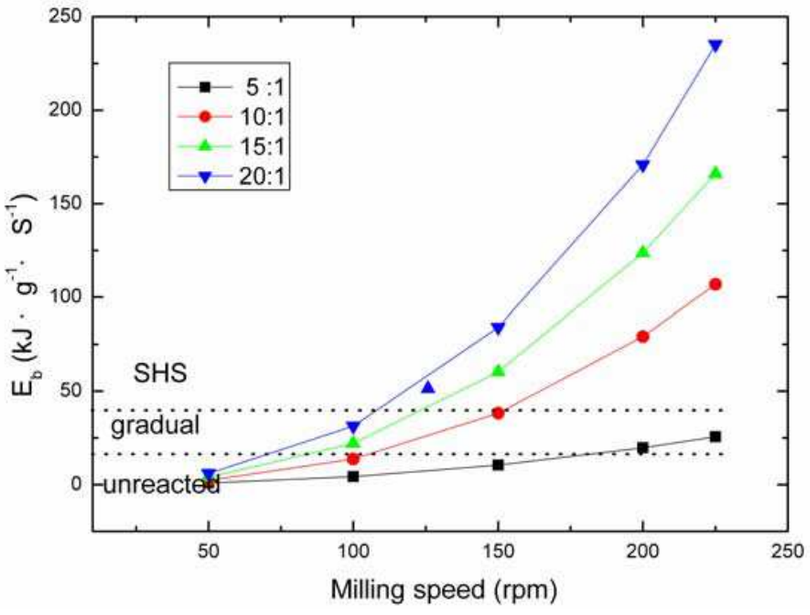


Fig. 3. Milling map of WC/MgO at different conditions

The relation between effective extensive factor (E_b) and total energy (E_t) can give an idea about the conditions required for gradual reaction and SHS mode during ball milling, as shown in Fig. 4. For WC/MgO synthesized through SHS mode the total energy value required is 25.61~61.82×10^6 kJ·g^{-1}, and for obtaining WC/MgO through gradual reaction, the total energy value required is above 112.83×10^6 kJ·g^{-1}, five times more than those powders fabricated with SHS reaction. The big difference in energy value for the two formation mode may be caused by the following reasons:

1. For an SHS mode, a small quantity of mixed powders trapped in the collision event could get enough energy to form WC/MgO first. The released combustion heat will be helpful for the following reactions. Therefore, the total milling energy required for the formation of WC/MgO can be maintained at a lower level.
2. For a gradual reaction mode, most of the milling energy has been used up in the diffusion process. Moreover, gradual reaction process needs much longer milling time, this means that heat loss is much serious. All the above discussions are based on the present collision model.

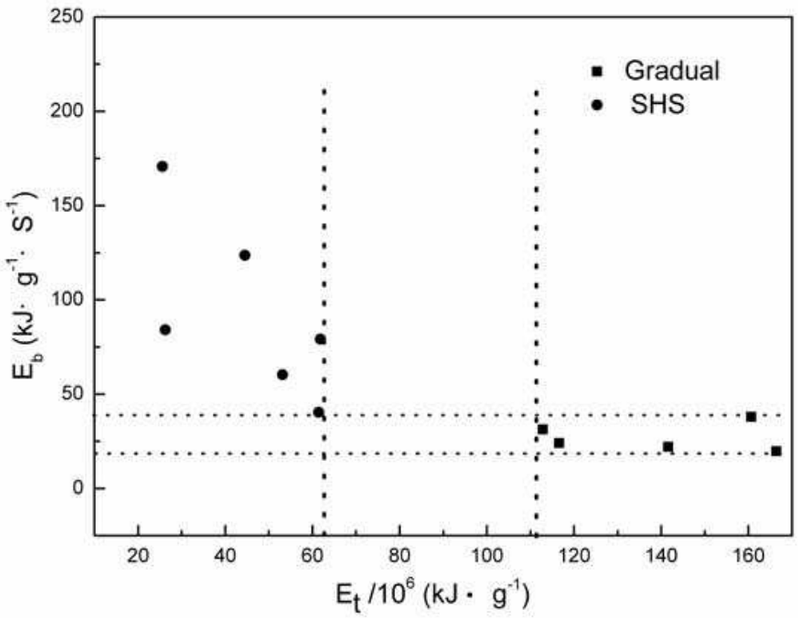


Fig. 4. Energy map of WC/MgO synthesized by SHS(●) and gradual (■) reaction

According to above analysis, a conclusion can be easily achieved that nanocomposite WC/MgO powders can be synthesized either by SHS or gradual reaction. In the present work, the milling energy is analyzed by using an improved model on the basis of Magini's and Yang's work, *i.e.* considering the multi-parameters that describe the energetics of the high-energy ball milling process. On the other hand, there still exist some defects, for instance, ignoring the loss of milling energy during which makes the calculated values higher than the actual ones. Whereas, based on the previous hypothesis that the impact energy is entirely absorbed by the powders, the milling maps are provided with predictive capability for choosing the proper milling conditions in the practical high-energy ball milling process.

2.3 Artificial neural network method application in MA process

Owing to the significant scientific and industrial importance of high-energy ball milling, considerable researches have been conducted on the process modeling, as stated previously, mainly based on the mechanistic (Abdellaoui & Gaffet, 1995; D'Incau et al., 2007; Chattopadhyay et al., 2001; Das et al., 1999; Abdellaoui & Gaffet, 1994) and thermodynamic (Badmos & Bhadeshia, 1997; Lu et al., 1997; Suryanarayana et al., 2001) approaches to achieve a great understanding at the atomic and phenomenological level. However, these models cannot be fully and accurately implemented due to the multi-influencing parameters, the inherent complexity and the oversimplified assumptions combined with the highly dynamic, non-linear behavior of a multi-physics and multi-scale nature (Feng, 2004).

Artificial neural network (ANN) is currently one of the most powerful modeling techniques based on a statistical approach, and it is suitable for simulations of correlations which are hard to be described by physical models (Sha & Edwards, 2007). Hence, the ANN technique is ideal for the intricate ball milling processes due to its utility to problems that involve the manipulation of multiple parameters and non-linear interpolation.

ANN provides a mapping of inputs to outputs and consists of computer programs based on the structure of brain. As such, they can be trained to recognize patterns within data. In the human brain, a neuron is a nerve cell which processes incoming information and outputs a signal to the relevant part of the body accordingly. Some inputs are stronger than the others, *i.e.* they are 'weighted'. The total effect of the inputs is the sum of the weighted signals, and, if this exceeds the neuron threshold, a response is produced. By comparison, in an ANN, a number of inputs are applied simultaneously, *via* weighted links, and the node calculates a combined total input. The relation between the input and output is specified by a transfer or activation function, which describes the threshold for deciding on the state of the output of that particular node. A number of nodes may be combined to form a layer, and layers may be interconnected to form a complete network. The detailed procedure of developing the ANN model for the synthesis of nanocomposite WC/MgO powders *via* high-energy ball milling process is described as follows.

2.3.1 Experimental data collection and processing

To develop an ANN with good performance, there needs an adequate quantity of experiment data available. The database was collected through the planetary ball milling experimental results. The experimental procedure is detailed described in (Ma et al., 2009). Constant milling time and atomic ratio of elemental powders were maintained throughout the series of experiments as detailed in previous.

The selection of the input parameters is very important for the ANN modeling. All relevant input parameters must be represented as the input data of the model. Among a number of parameters involved in the ball milling process, the variables, including milling speed (v), ball diameter (d_B) and ball-to-powder weight ratio (R_{BP}) have been chosen as the input parameters. The morphology of the as-milled powders, characterized by crystallite size (d), specific surface area (S) and median particle size (d_{50}), were the individual output for three separate back-propagation (BP) network models.

In total, 96 input/output data pairs for training the neural network were formed on the basis of the experiments, and the remaining 16 pairs were reserved for testing the performance of the trained network. The ranges of the numerical values of the network

input and output are listed in Table 3. These data was converted and normalized to a suitable form for use with the ANN by

$$v' = \frac{v - \min_a}{\max_a - \min_a}\left(new\max_a - new\min_a\right) + new\min_a \tag{10}$$

where v' is the pattern vector, v is the value of a certain variable (it can be v, d_B or R_{BP}, etc.), max_a and min_a are the maximum and minimum values of the independent variable. Additionally, "1" is its new maximum value ($newmax_a$), and "-1" is the variable's new minimum value ($newmin_a$).

Data	Variable	Values		Mean value	Standard deviation
		Maximum	Minimum		
Input	V (r/min)	350	200	275	64.550
	d_B (mm)	10	4	7	2.582
	R_{BP}	10	4	7	2.582
Output	d (nm)	35.173	19.876	26.767	4.295
Output	S (m^2g^{-1})	7.690	0.799	3.791	2.241
Output	d_{50} (μm)	7.842	0.703	2.276	2.226

Table 3. Range of the numerical values of the neural network input and output data

2.3.2 Neural network training and its performance

The process of fitting the network to the experimental data is called *training*. During its training phase, the network was repeatedly presented with a set of training patterns, comprising input-output pairs, until either the output error was minimized to a satisfactory level (0.001) or the maximum number of training cycles was reached. On completion of the training, a set of previous unused patterns were applied to the network inputs, here without example outputs. In this way the ability of the network to classify the composites' characteristics on the basis of new information was tested.

The back-propagation (BP) network architecture was selected and applied. It includes an input layer, which just propagates input values to the nodes of the hidden layer, a single hidden layer and an output layer. The employed BP network algorithm is available inside the Neural Network Toolbox (Version 4.0.1), MATLAB® 7.1 (14th release).

In order to determine number of the hidden nodes in the network, several BP networks with various hidden nodes (max to 24 nodes) are considered and the corresponding mean square of the network errors (MSE) are calculated by

$$E(w,B) = \frac{1}{N}\sum_{i=1}^{N}\left(t_k - a_k\right)^2 \tag{11}$$

where N is the total number of training patterns, t_k is the target/desired value, and a_k is the network output value.

Fig. 5 demonstrates that the number of neurons in the hidden layer for crystallite size model, specific surface area model and median particle size model is 15, 13 and 16 correspondingly, which yield the minimum mean square error for training dataset. As a result, Table 4 lists the specifications of the architecture of the selected neural network.

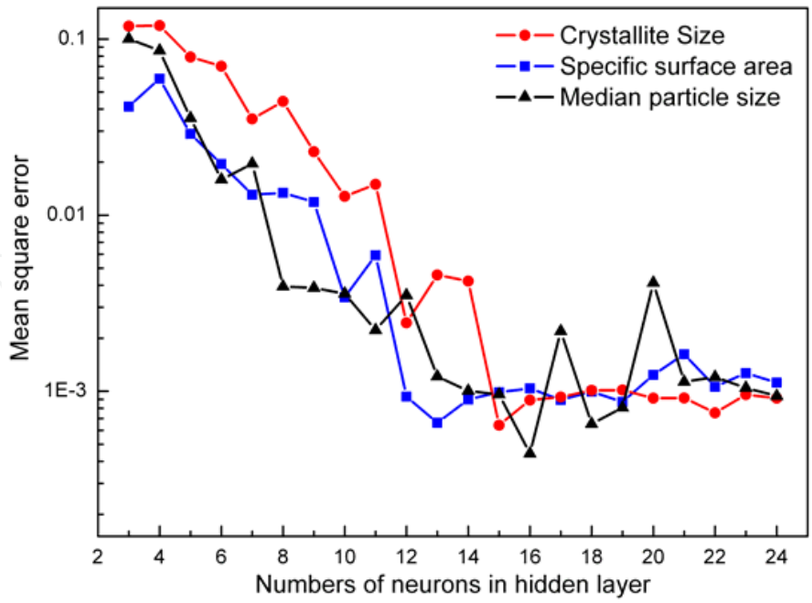


Fig. 5. Mean square errors of different BP neural networks with different neurons in the hidden layer

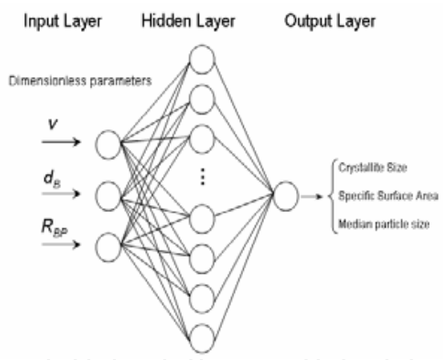
Parameters	BP network type	Diagram
Numbers of input layer	1	
Numbers of hidden layer	1	
Numbers of output layer	1	
Numbers of inputs	3	
Numbers of neurons in hidden layer for crystallite size	15	
Numbers of neurons in hidden layer for specific surface area	13	
Numbers of neurons in hidden layer for median particle size	16	
Numbers of outputs	1	
Activation function	Tangent-sigmoid	

Table 4. Specifications of the BP neural network design

The performance accuracy of the network can be checked by the error of neural network predictions. For the test dataset, neural network predictions are calculated. These are compared with the corresponding experiment values. Thereafter, the relative errors are calculated using

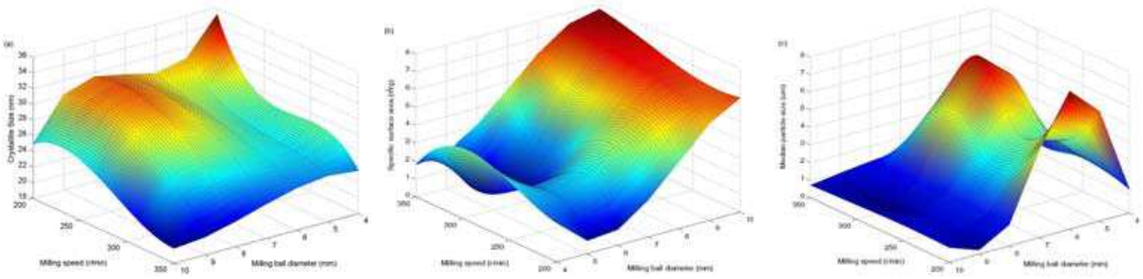
$$Error = \frac{Rm_{EXP} - Rm_{NN}}{Rm_{EXP}} \times 100\% \tag{12}$$

where Rm_{EXP} is the experimental (measured) crystallite size, specific surface area and median particle size, and Rm_{NN} is the predicted values from the neural network.

The average absolute relative error for the *predictions* of crystallite size, specific surface area and median particle size is 8.22%, 7.88% and 4.05% respectively. They are not too bad, considering the limited amount of training data available and large error prone to X-ray measurements of crystallite size and laser measurement of specific surface area and median particle size. These acceptable performances achieve a result that our BP network model can predict with sufficient accuracy for the practice.

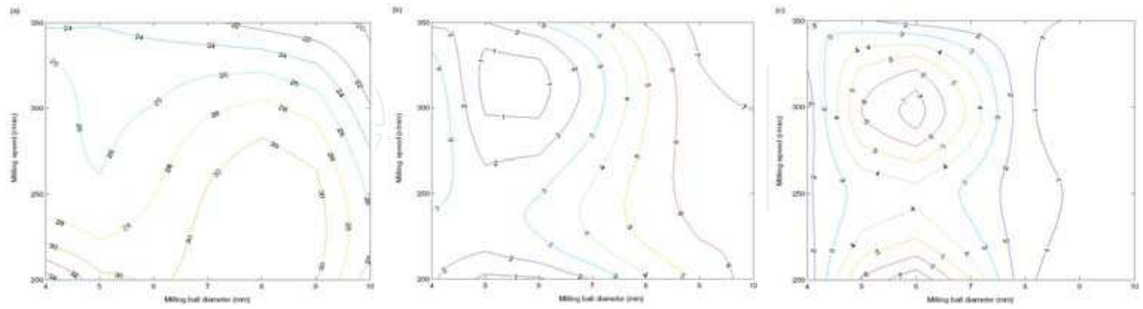
2.3.3 Neural network applications in powder property studies

After the above accuracy evaluation and prediction, the neural network technique can be further applied to the optimization of the ball milling process for fabricating the nanocomposite WC/MgO powders. Fig. 6 shows the response surfaces of powder properties, obtained by BP network models, with the milling parameters. Note that only two ball milling parameters (milling speed and milling ball diameter) are discussed in the present optimization for the reason that the remaining variable (ball-to-powder weight ratio) is mainly affected by the milling time which is maintained as a constant value. According to the research of (Suryanarayana, 2001), ball-to-powder weight ratio can no longer be considered with the certain milling time in the current optimization.



(a) (b) (c)

Fig. 6. Surface responses of crystallite size (a), specific surface area (b) and median particle size (c) of the milled powders vs. the milling parameters obtained by ANN technique



(a) (b) (c)

Fig. 7. Contour plots of crystallite size (a), specific surface area (b) and median particle size (c) of the milled particles vs. the milling parameters v and d_B

As to the clarification of the response surfaces, the contour plots for those properties are demonstrated in Fig. 7. Variations of the crystallite size, specific surface area and median particle size in the response surfaces could be confirmed with the theories reported by many

other researchers (Suryanarayana, 2001; Calka & Radlinski, 1991; Lai & Lu, 1998; Watanabe et al., 1991). It is widely understood that the faster the mill rotates the higher would be the energy input into the powder. At high milling speeds (or intensity of milling), the temperature of the vial may reach a high value which may be advantageous in the current case where diffusion is required to promote homogenization and/or alloying in the WC powders. Additionally, the size of the grinding medium (milling ball diameter) also has an influence on the milling efficiency. Generally speaking, a large size (and high density) of the milling ball is useful since the larger diameter/weight of the balls will transfer more impact energy to the powder particles.

In a word, the results achieved by the surface responses and contour plots indicate that a consistent agreement exists among the outcomes of ANN modeling, the above theoretical description and the experimental implementation. Therefore, the response surfaces and contour plots can be applied to the optimization of the ball milling process of fabricating the nanocomposite powders. The nanostructured WC/MgO powders posses the excellent morphological characteristics, such as homogeneous shape with fine and smooth surface relief and uniform size (less than 0.8 μm in diameter). These powders will be consolidated into the bulk materials for the further industrial application. On the basis of the contour plots and current experimental circumstances, the optimized milling parameters (300r/min<v≤350r/min and 8mm≤d_B≤10mm) can be obtained using this series model of BP neural network.

2.4 Process control agent

As mentioned above, the mechanochemical reaction among WO_3, Mg and C reactant powders to form nanocompostite WC/MgO powders can be the SHS one. However, dangerous explosion caused by SHS may occur abruptly, which is difficult to control. In addition, a significant portion of coarse WC/MgO crystallites and particles may form due to particle melting under the high temperature caused by SHS. Furthermore, the powder yield is low as many particles get adhere to the milling balls and vial, which is difficult to be detached.

There are two possible methods to prevent the combustion reaction and the severe welding, one is to lower the temperature of the milling vial (Jang & Koch, 1990; Guo et al., 1990; Fecht et al., 1990), and the other is to add stearic acid as a process control agent (PCA) to the reactant powders (Suryanarayana & Sundaresan, 1991; Wang et al., 1991). The effects of stearic acid on the ball milling process of CuO-Ca/Ni, Ti-BN and Al-Mg systems had been investigated by Schaffer, Byun and Lu respectively (Schaffer & McGormick, 1990; Byun et al., 2004; Lu & Zhang, 1999). Results show that with the addition of stearic acid, the occurrence of combustion reaction can be successfully delayed or suppressed, the inter-particle welding during collisions can be inhibited, and the particle size can be decreased. It may be noted that a combustion reaction should be avoided if one is interested in producing the materials in nanocrystalline state. This is because combustion may result in partial melting and subsequent solidification will lead to the formation of a coarse-grained structure. Another requirement for formation of nanometer-sized particles is that the volume fraction of the by-product phase must be sufficient to prevent particle agglomeration (Suryanarayana, 2001).

The reactant WO_3-Mg-C mixture was charged together with steatic acid (99.9%, flaky) and hard alloy balls (10 mm in diameter) into a hard alloy vial (250 ml in volume). The amount

of stearic acid was controlled from 0 to 2.0 wt. %. More experimental details can be found in (Wu et al., 2010).

2.4.1 Effect of stearic acid on the mechanochemical reaction

As stated above, only the WO_3, Mg and C peaks could be detected in the initial 5 h of ball milling (Fig. 1). When milling for 4.7 h, the WO_3-Mg-C mixture abruptly reacted to form WC/MgO. Slight explosion sound could be heard during milling for 4.7 h, and the temperature of the milling vial reached an evidently high level almost at the same time, as shown in Fig. 8a. These phenomenons indicate that the occurred reaction (1) is a mechanically induced self-propagating reaction. Fig. 8b shows the TEM micrograph for the agglomerated powder which resulted just after the temperature peak. The particles in Fig. 8b are very coarse and most of the size is above 100 nm.

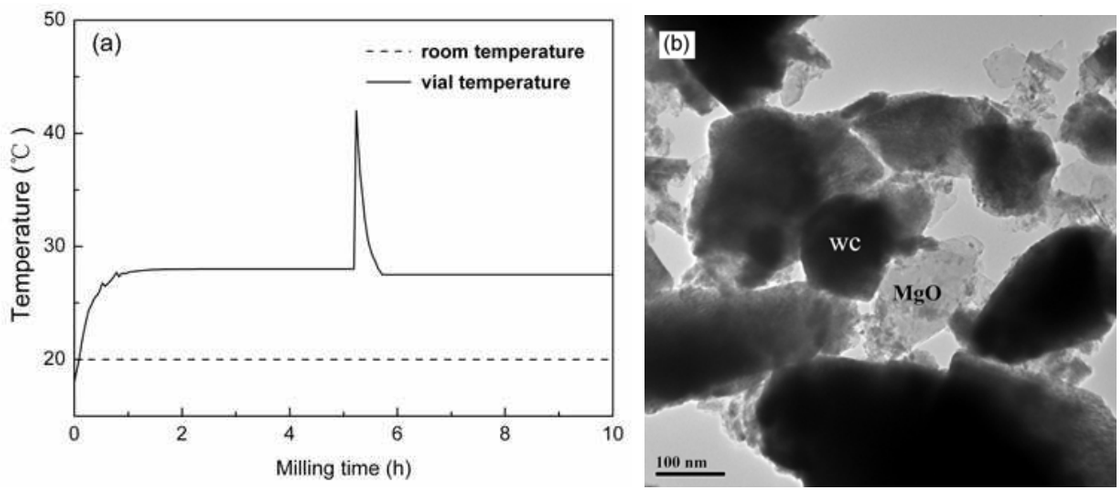


Fig. 8. (a) Temperature vairation of milling vail during milling for reaction (1) and (b) the corrisponding TEM micrograph

The SHS, completes within a very short time, however, it always results in the occurrence of dangerous explosion phenomenon and the formation of coarse WC/MgO particles. With the aim of preventing SHS, stearic acid is added as a PCA. Fig. 9 indicates that the incubation time (the time from the beginning of milling to the occurrence of SHS) for the SHS depends on the concentration of stearic acid. The incubation time is about 5.5 h without stearic acid and there are little changes up to 0.8 wt. % of stearic acid. The addition of stearic acid of between 1.1 and 1.2 wt. % further increases the incubation time, but the SHS still occur. When 1.2 wt. % of stearic acid is added, however, the SHS is suppressed in two experiments while it occurs in another two. With over 1.2 wt. % of stearic acid, reaction (1) always proceeded gradually. Therefore, the critical concentration of stearic acid to inhibit the SHS of reaction (1) is about 1.2 wt. %.

Fig. 10 shows the XRD patterns of the powders with different amounts of stearic acid after 80 h milling. When the concentration of stearic acid is lower than 1.2 wt. %, there is no distinct difference in the XRD patterns of the powders, as shown in Figs. 10a, b and c. However, it can be found from Figs. 10d and 10e that with over 1.2 wt. % of stearic acid, both WC and MgO peaks broaden much more, which means that the suppression of SHS contributed to the reduction of the crystallite size and the increase of mircostrain. The

average crystallite sizes of WC and MgO, estimated by formula in (Chakurov et al., 1987), are 19 and 29 nm without stearic acid, and 10 and 15 nm with 1.4 wt. % of stearic acid respectively, under the same milling conditions. Nevertheless, with over 2.0 wt. % of stearic acid, WC/MgO can't be successfully formed even ball milling for over 100 h, as shown in Figs. 10f and 10g.

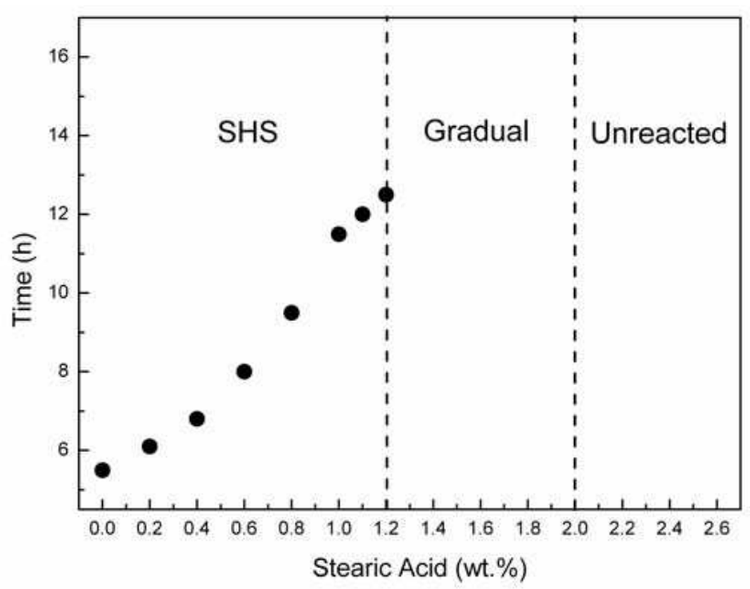


Fig. 9. Incubation time for SHS with different amount of stearic acid

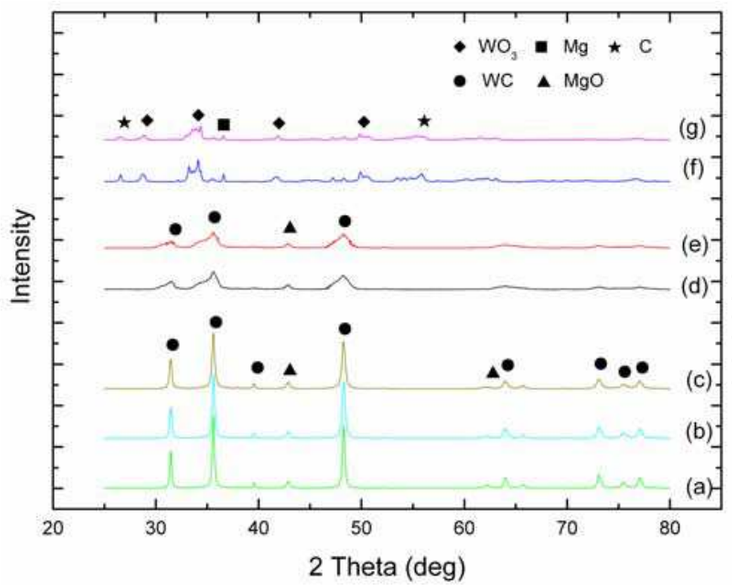


Fig. 10. XRD patterns of powders milled for 80 h with (a) 0, (b) 0.8, (c) 1.1, (d) 1.4, (e) 1.8, (f) 2.0 and (g) 2.2 wt.% of stearic acid

The above results indicate that the critical concentration of stearic acid to change reaction (1) from SHS to a gradual reaction is about 1.2 wt. %. In general, the change of reaction mode

by an inert addictive is attributed primarily to two mechanisms, i.e. increasing the heat capacity and decreasing the contact area between the reactants (Takacs, 2002; Chakurov et al., 1987). Munir (Munir, 1988) proposed a simple guideline to decide whether or not a self-propagating reaction might occur for a certain system. According to his proposal, the reaction can start without additional energy from an exterior source when the adiabatic temperature rise ($-\Delta H/C_p$) is above 2000 K. The $-\Delta H/C_p$ of reaction (1) calculated from the thermodynamic date will decrease from ~ 6000 K to ~ 5800 K, under which the SHS would still occur. Thus, it seems that the suppression of the SHS by stearic acid is primarily owing to the decrease in contact area among the reactants. The stearic acid, being absorbed on the surface of reactant powders, helps decreasing the contact area among them, which leads to the slowing down of the reaction rate and therefore either delays or completely suppresses the SHS. However, the contact area may be too little to initiate reaction (1), if excessive (>1.8 wt. %) stearic acid absorbed on the surface of reactant powders. It should be noted that such an amount is too small to consider the possibility that change the reaction mode could be induced by other reactions, as there is no other phase can be observed in the XRD patterns, as shown in Fig. 10.

2.4.2 Effect of stearic acid on the microstructure of powders

With the aim to investigate the effect of stearic acid on the microstructure of the mechanical alloyed powders, the powders milled with 0 wt. %, 1.1 wt. %, and 1.4 wt. % of stearic acid for 80 h are characterized by TEM, as shown in Fig. 11. These three powder samples all contain two phases: the first phase WC appears as deep-black grains, while the second phase MgO consists of light-gray grains. Fig. 11a indicates that the crystallite size of WC and MgO milled without stearic acid is rather large and unhomogeneous, in great part are above 50 nm, even approaches to 100 nm. The crystallite size of powders milled with 1.1 wt. % of stearic acid can be a little decreased and its homogeneity of particle size can be slightly improved either, as shown in Fig. 11b. The reaction mode can be changed from SHS to a gradual one when the concentration of stearic acid is increased to be 1.4 wt. %. Fig. 11c shows that there are no such large crystallites and the sizes of the homogeneously distributed WC and MgO crystallites are much smaller, mostly are between 10 and 25 nm. Thus, the average crystallite size and agglomeration can be considerably decreased and the homogeneity of particle size can be obviously improved when the amount of stearic acid is enough to suppress the occurrence of SHS.

During high-energy ball milling process, considerable plastic deformation of powders greatly enhance the surface activity, thus the neighboring powder particles may get together to reduce the surface activity, which can hinder the refinement and mechanical alloying of the processing powders. When an appropriate amount of stearic acid is added into the reactant powders during ball milling, stearic acid will adsorb onto the fresh surface to decrease the surface activity and inhibit the conglomeration of powders, because adsorption is a free energy self-decreasing process. Fig. 11 suggests that the microstructure of powders can be improved with the addition of stearic acid, however, there is no obvious effect unless the amount of stearic acid is enough to change the reaction mode from a SHS to a gradual reaction. This can be expressed by the reason that the vial surface temperature may be maintained at a low level during the synthesis process of WC-MgO through steady gradual reaction, which is in favor of obtaining homogeneously distributed fine particles and crystallites. While the vial surface temperatures may reach a high value due to the excessive

combustion heat liberated during SHS process, and these temperatures lead to the melting, consolidation and formation of large particles of the reaction products.

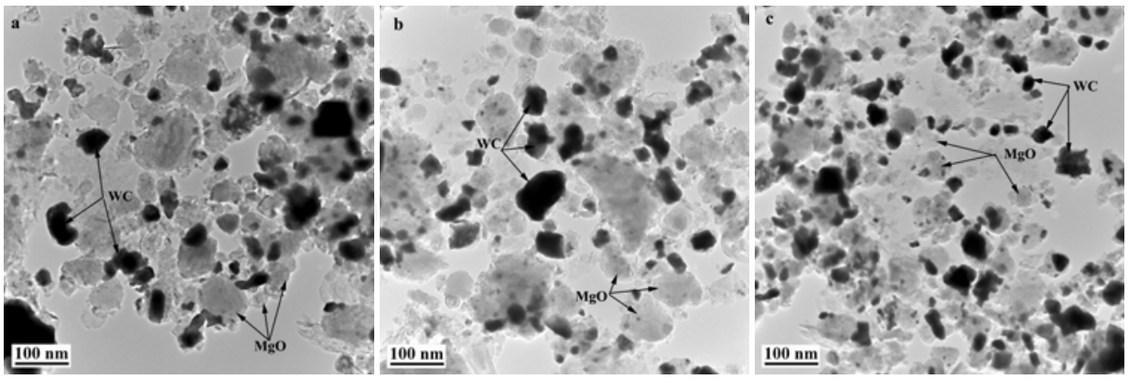


Fig. 11. TEM pictures of powders milled for 80 h with (a) 0 wt. %, (b) 1.1 wt. %, (c) 1.4 wt. % of stearic acid.

2.4.3 Effect of stearic acid on the powder yield of powders

Powder yield is one of the most important indicators to estimate as-milled powders recovered after ball milling, which is commonly expressed by the ratio between the weight of powders after and before ball milling. Powder yield also can quantificationally reflect the adhering degree of powders during mechanical alloying. Fig. 12 shows the relation between powder yield and the amounts of stearic acid added.

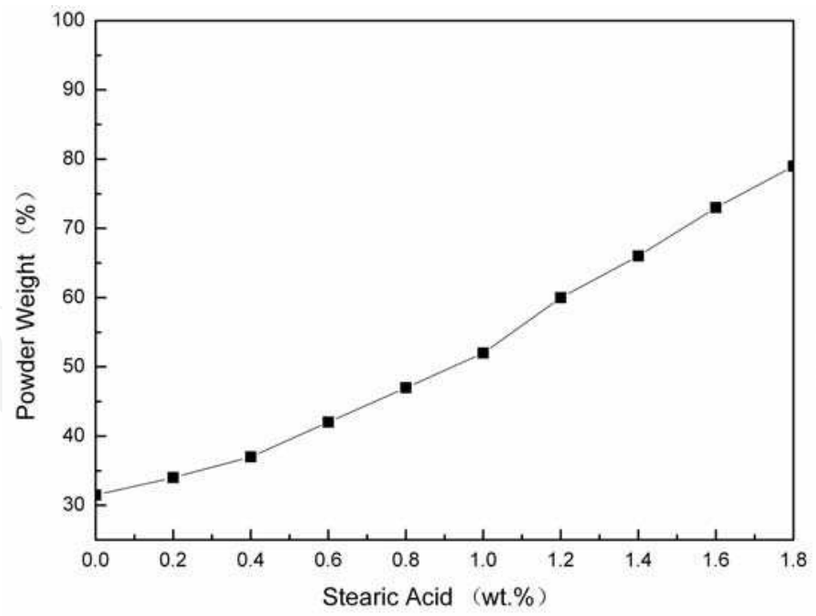


Fig. 12. Relation between powder product yield and the amounts of stearic acid added

It can be found by Fig. 12 that the powder yield can be greatly enhanced to be 80.6 % when 1.8 wt. % of stearic acid is added, as other milling parameters are maintained at the same value. After 80h of ball milling, fine WC-MgO powders can be obtained, and both the

surfaces of vial and milling balls are bright and clean, nearly no adhering phenomenon can be observed. On the other hand, the powder yield is rather low (31.5 %) when milled without stearic acid under the same milling conditions. The end powders exhibit with large grain size, and a great quantity of powders get coated onto the surface of the milling balls and vial. While no WC-MgO powders can be formed when over 1.8 wt. % of stearic acid is added, therefore the powder yield under this milling condition haven't been further discussed and investigated.

During ball milling process, constant collisions among milling balls, powders and milling vial result in the plastic deformation of the powders. Small parts of powders get cold welded onto the milling balls and vial, while a great part of powders particles are refined by work-hardening. Due to the increase of the surface activity, the refined powders will be inclined to get together and coated onto the milling balls and vial spontaneously. This is a process in which the free energy gets decreased. Therefore, the adhering of powders to the milling balls and vial is unavoidable when milled without stearic acid. A very thin "protective film" between the powders and the milling balls/vial may form with the addition of stearic acid. This "protective film" prevents the contact between the powders and the milling balls/vial, which decreases the abrasion induced by milling balls, as well as reduces the adhering of powders to the milling media. Moreover, the adsorption of stearic acid on the powder surface can also decrease the surface energy of powder particles, and diminishes the adsorption driving force of powders to the milling balls and vial, consequently reduces the possibility of adhering of powders to the milling balls and vial. As a result, the addition of stearic acid can greatly increase the powder yield, which is an important method to overcome the adhering problem during the process for synthesizing nanocomposite WC/MgO powders.

3. Consolidation of nanocomposite WC/MgO powders

Sintering behavior of nanocomposite WC/MgO powders and its consolidated bulk properties are studied. The as-milled WC/MgO powders were sintered by plasma-activated sintering (PAS) and hot-pressing sintering (HPS) at the same sintering conditions, *i.e.* maximum temperature: 1650 °C, applied pressure: 40 MPa. The microstructures were analyzed and compared in order to understand the influence of the two sintering techniques. The density of the consolidated samples and the following mechanical properties were measured: Vicker hardness and the estimated fracture toughness.

The XRD pattern of the WC/MgO powders and the consolidated sample *via* PAS and HPS method were shown in Fig. 13. The strong diffraction peaks of WC (hexagonal structure) and MgO (cubic structure) were clearly observed. Thus, it indicated the hot-pressing sintered bulk materials were mainly composed of the WC and MgO phases. W_2C phase was detected in the sintered bulk, but its intensity in the HPS sintered sample was greater than those of the PAS one, which may be due to the decarburization phenomena during sintering.

Fig. 14 presents the microstructures of the polished samples sintered by HPS and PAS at 1650 °C. The energy dispersive spectroscope (EDS) analysis reveal that the dispersed white particulates were composed of the Mg and O elements, while the surrounding dark matrix was rich in W and C element. Combined with XRD results (Fig. 13), it is reasonable to

conclude that the composites of WC matrix with the MgO particulates toughened can generally be produced. However, the dispersion states of the toughening particulates were significantly influenced by the sintering method. In the sample sintered by HPS, the MgO showed an irregular polygonal shape and were larger than 2 μm in size (Fig. 14a). Compared with that, the toughening particulates in the bulk consolidated by PAS were presented in a refined and dispersed morphology (Fig. 14b).

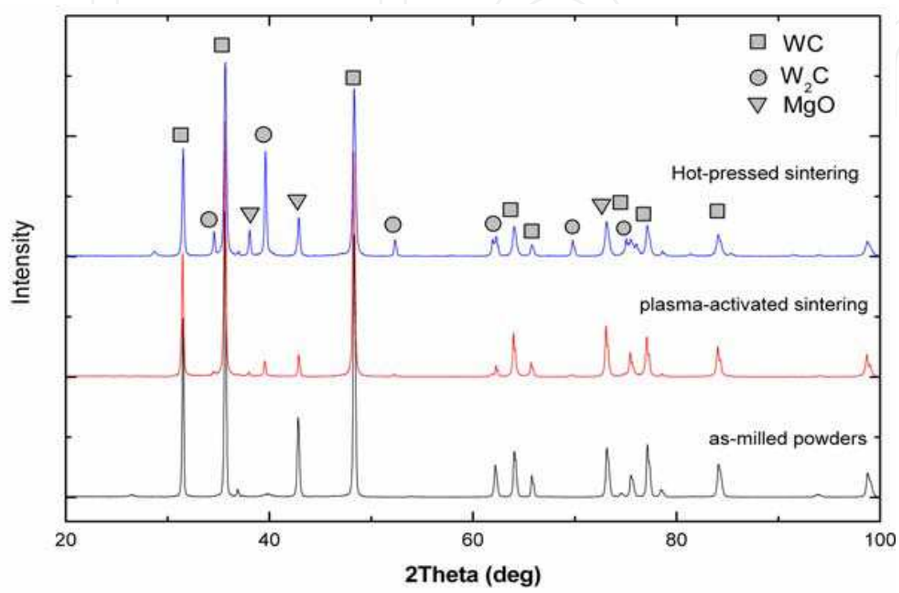


Fig. 13. XRD pattern of the end-powders and the consolidated WC/MgO bulk

HPS consolidation of WC/MgO powders resulted in an agglomeration of MgO particulates and pores in the matrix (Fig. 14a), leading to a relatively low bulk densification of 94.56 % theoretical density (T.D.). Sintered by PAS, the refined MgO toughening particulates were homogeneously distributed in the matrix, showing very little aggregation (Fig. 14b). In this instance, a relatively high densification response of 99.3% TD was obtained (Table 5).

Sintering Method	Relative Density/ %	Vickers Hardness (HV/GPa)	Fracture Toughness (K_C/MPa·m$^{1/2}$)
Hot-pressing sintering (HPS)	94.56	15.43	9.58
Plasma-activated sintering (PAS)	99.3	17.78	12.21

Table 5. Some measured mechanical properties of the fabricated bulk materials via HPS and PAS

Table 5 also depicts the hardness and fracture toughness measured on the polished sections. It is clear with the HPS method, the hardness was about 15.43 GPa and the estimated fracture toughness was 9.58 MPa•m$^{1/2}$. This can be attributed to the pores distribution and significant MgO agglomeration segregation throughout the sintered structure. The hardness of the sample sintered by PAS was measured to be 16.65 GPa, taking the average of at least

10 indentations. The resulting indentation cracks were used as the indication of the fracture toughness (K_c) *via* the model that was suggested by Shetty et al (Shetty et al., 1985). We should note that the Vickers hardness measurements that were made are a rough approximation for the valid K_c test. Hence, they were an approximation of the expected fracture toughness measurements. In a word, the overall mechanical performance of the HPS sintered sample was lower than those of the PAS sintered one. But this indicates the possibility of preparing high-hardness and high-fracture-toughness composite materials.

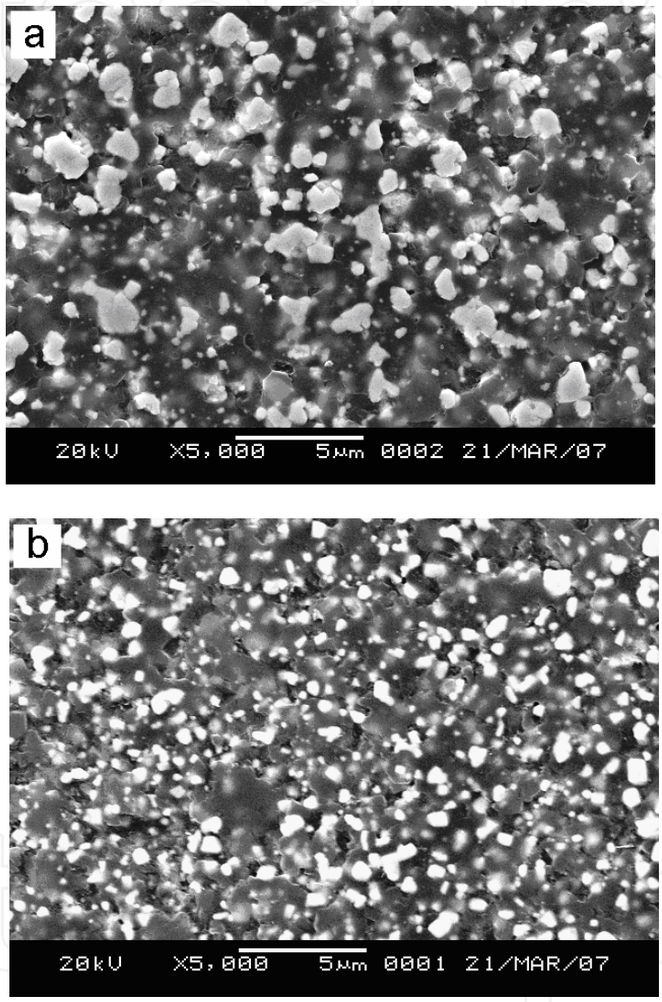


Fig. 14. Backscattered micrographs of polished surfaces of the samples sintered by (a) HPS and (b) PAS

As stated above, WC/MgO composite can be a new advanced hard refractory material. In Table 6, we provide a comparison of the hardness and fracture toughness values of WC/MgO compacts with those of WC-Co reported by others (Richter & Von Ruthendorf, 1999; Almond & Roebuck, 1988; Kim et al., 2007). It can be seen that the hardness and fracture toughness of WC/MgO is comparable with the value reported in other literatures. The hardness and fracture toughness value of the WC/MgO sample produced by PAS had the highest values, and is as good as the samples with a metallic binder. In contrast to those

microns- and submicrons-grained structure of WC-Co composites, the nanocomposite WC/MgO material has offered unique properties of superior hardness and toughness combination. It is reasonable to propose WC/MgO as a new industrial material.

Reference	Materials	Sintering method	*HV* (GPa)	K_C (MPa·m$^{1/2}$)
(Richter & Von Ruthendorf , 1999)	WC-10 wt. %Co	PAS	17.64	6
(Almond & Roebuck, 1988)	WC-10 wt. %Co	PAS	13.06	13.5
(Kim et al., 2007)	WC-10 wt. %Co	PAS	17.21	11.6
(Kim et al., 2007)	WC-12 wt. %Co	PAS	17	12.2
This study	WC-MgO	HPS	15.43	9.58
This study	WC-MgO	PAS	17.78	12.21

Table 6. Comparison of mechanical properties of the consolidated WC/MgO bulks and WC-Co with previously reported values

4. Summary

Nanocomposite WC/MgO powders can be successfully synthesized by high-energy planetary ball milling a powder mixture of WO_3, graphite and Mg under room temperature. This technique has a great advantage because it not only overcomes the deficiency of high cost in fabricating WC under high temperature, but replaces the noble metal cobalt with MgO as well.

Studying the mechanism involved in the synthesis, we find that mechanical alloying processing can agitate the reaction mass and continually bring unreacted materials into contact, preventing the products from dividing the reactants separately. This results in a significant increase in reaction rate which provides the occurrence of WC/MgO formation at ambient temperature.

Combined the formation mode with the milling conditions, the milling energy maps for preparing nanocomposite WC/MgO powders by high-energy planetary ball milling are established. Self-propagation high-temperature synthesis reaction (SHS) and gradual reaction are two kinds of formation mode of WC/MgO at different milling conditions. The energy region for gradual reaction and SHS is defined, *i.e.* when the effective extensive factor E_b is above 38.24 kJ·g^{-1}·s^{-1}, the reaction mode is SHS; it is the gradual reaction when E_b is 22.12~38.14 kJ·g^{-1}·s^{-1}; the formation of WC/MgO cannot be achieved when E_b is below 22.12 kJ·g^{-1}·s^{-1}. For SHS, the excessive heat released and high temperature rise during the abruptly occurred reaction make the process difficult to control. The milling energy maps also help to predict capability for fabricating WC/MgO through gradual reaction by adjusting the milling parameters appropriately.

It can be concluded that ball milling is an inherently complex process due to the multi-influencing parameters. Fortunately, neural network technique (NN) can be the ideal modeling for this highly complicated and non-liner high-energy planetary ball milling process. The BP network is selected since this feed-forward multilayer network is further fully connected. The architecture of the BP network models can be implemented: a) The series model of BP network is designed to be "3-*n*-1", *i.e.* it includes one input layer which contains the ball milling variables (milling speed, ball-to-powder weight ratio and milling

ball diameter), one hidden layers (with different number of nodes [n] for different model) and one output layer which indicates the morphological characteristics of the WC/MgO powders (crystallite size, specific surface area and median particle size respectively). b) The tangent-sigmoid function is found to be the transfer activation. c) The number of neurons in the hidden layer (n) is 15, 13 and 16 for crystallite size model, specific surface area model and median particle size model individually, which is selected according to the mean square error of BP network calculations. The viability of the model is confirmed by the network prediction errors analysis. The results from the BP network prediction perform a good coherence with the experimental data. Furthermore, the optimization of the ball milling process for fabricating the nanocomposite WC/MgO powder is carried out through the analysis on the evaluated network response surface and contour plots. The optimized milling parameters (300 r/min < v ≤ 350 r/min and 8 mm ≤ d_B ≤ 10 mm) can be obtained through the ANN model and the present experimental details. Accordingly, the BP neural network technique can be applied to the high-energy planetary ball milling process with its high reliable performance and practical significance.

In the course of ball milling, the powder particles may cold-welded to each other due to the heavy plastic deformation among them. The true alloying among powder particles can occur only when a balance is maintained between cold welding and fracturing of particles. Regarding this, a process control agent (PCA) is usually added to the powder mixture during milling to reduce the effect of cold welding. Herein, stearic acid is added as a PCA to the reactant powders. The effects of stearic acid and its amount on the WO_3-Mg-C ball milling process, the microstructure evolutions and powder yield rate of WC/MgO have been investigated. The results show that the crystallite and particle sizes of WC/MgO powders can be refined, the homogeneity of particle size can be improved and the powder yield can be enhanced with the addition of stearic acid as a PCA. Furthermore, the mechanochemical reaction among WO_3, Mg and C reactant powders to form nanocompostite WC/MgO powders can be changed from a SHS mode to a gradual reaction by adding over 1.2 wt. % of stearic acid. The WC/MgO powders synthesized through gradual reaction are possessed of finer crystallites and more homogenous particle size distribution. Compared with the unstable and dangerous SHS, the steady and controllable gradual reaction is more suitable to be applied to the practical production.

The as-milled WC/MgO powders are sintered by plasma-activated sintering (PAS) and hot-pressing sintering (HPS) at the temperature of 1650 °C with applied pressure of 40 MPa. The relative density, hardness and fracture toughness of the compacted samples are tested. Results indicate that PAS is an attractive technique that the sintering procedure takes place in a short period of time (consolidation is achieved within a few minutes, 5 minutes). According to the microstructure observation, grain growth of the bulk samples can be minimized and the sintered compacts maintain their unique properties, i.e. superior hardness (HV = 17.78 GPa) and toughness (K_c = 12.21 MPa·m$^{1/2}$) combination.

Another important factor in the course of sintering that conquers the grain growth of the bulk samples and uniforms the toughening particulates (MgO) dispersion is the source of the milled WC/MgO powders. When the as-milled WC/MgO powders, which are introduced to the consolidation, have homogeneous shape with fine nanocrystalline grains, the PAS sintering may result in formation of full dense compacts (99 % T. D.). It is worth noting that PAS technique does not form any undesirable reactive products such as W_2C. In conclusion, the composite WC/MgO, which achieves competitive values of hardness and fracture toughness, can be an ideal engineering material as the alternative of WC-Co.

5. References

Abdellaoui, M. & Gaffet, E. (1994). Mechanical alloying in a planetary ball mill-kinematic description. *Journal de Physique IV*, 4, 291-296, ISSN: 1155-4339

Abdellaoui, M. & Gaffet, E. (1995). The physics of mechanical alloying in a planetary ball mill: mathematical treatment. *Acta Metallurgica Materialia*, 43, 1087-1098, ISSN: 0956-7151

Almond, E. A. & Roebuck, B. (1988). Identification of optimum binder phase compositions for improved WC hard metals. *Materials Science and Engineering A*, 105/106, 237-248, ISSN: 0921-5093

Badmos, A. Y. & Bhadeshia, H. K.D. H. (1997). The evolution of solutions: a thermodynamic analysis of mechanical alloying. *Metallurgical and Materials Transactions A*, 28, 2189-2194, ISSN: 1073-5623

Benjanmin, J. S. (1970). Dispersion-strengthened superalloys by mechanical alloying. *Metallurgical and Materials Transactions*, 1, 2943-2951, ISSN: 1073-5615

Burgio, N.; Iasonna, A.; Magini, M.; Martelli, S. & Padella, F. (1991). Mechanical alloying of the Fe-Zr system. Correlation between input energy and end products. *Il Nuovo Cimento D*, 13, 459-476, ISSN: 0392-6737

Byun, J. S.; Shim, J. H. & Cho, W. Y. (2004). Influence of stearic acid on mechanochemical reaction between Ti and BN powders. *Journal of Alloys and Compounds*, 365, 149-156, ISSN: 0925-8388

Calka, A. & Radlinski, A. P. (1991) Universal high performance ball-milling device and its application for mechanical alloying. *Materials Science and Engineering A*, 134, 1350-1353, ISSN: 0921-5093

Chakurov, Kh.; Rusanov, V. & Koichev, I. (1987). The effect of inert additives on the explosive mechanochemical synthesis of some metal chalcogenides. *Journal of Solid State Chemistry*, 71, 522-529, ISSN: 0022-4596.

Chattopadhyay, P. P.; Manna, I. & Talapatra, S. (2001) A mathematical analysis of milling mechanics in a planetary ball mill. *Materials Chemistry and Physics*, 68, 85-94, ISSN: 0254-0584

Das, D.; Chatterjee, P. P. & Manna, I. (1999). A measure of enhanced diffusion kinetics in mechanical alloying of Cu-18 at. % Al by planetary ball milling. *Scripta Materialia*, 41, 861-866, ISSN: 1359-6462

D'Incau, M.; Leoni, M. & Scardi, P. (2007). High-energy grinding of FeMo powders. *Journal of Materials Research*, 22, 1744-1753, ISSN: 0884-2914

Doppiu, S.; Schultz, L. & Gutfleisch, O. (2007). In situ pressure and temperature monitoring during the conversion of Mg into MgH_2 by high-pressure reactive ball milling. *Journal of Alloys and Compounds*. 427, 204-208, ISSN: 0925-8388

Fecht, H. J.; Hellstern, E.; Fu, Z. & Johnson, W. L. (1990) Nanocrystalline metals prepared by high-energy ball milling. *Metallurgical and Materials Transactions A*, 21, 2333-2337, ISSN: 1073-5623

Feng, Y. T.; Han, K. & Owen, D. R. J. (2004). Discrete element simulation of the dynamics of high energy planetary ball milling processes. *Materials Science and Engineering A*, 375, 815-819, ISSN: 0921-5093

Gessinger, G. H. (1976). Mechanical alloying of IN-738. *Metallurgical and Materials Transactions A*, 7, 1203-1209, ISSN: 1073-5623

Gleiter, H. (1989). Nanocrystalline materials. *Progress in Materials Science*, 33, 223-315, ISSN: 0079-6425

Guo, W.; Martelli, S.; Burgio, N.; Magini, M.; Padella, F. & Paradiso, E. (1990). Mechanical alloying of the Ti-Al system. *Journal of Materials Science*, 26, 6190-6196, ISSN: 0022-2461

Jang, J. S. C. & Koch, C. C. (1990). The hall-petch relationship in nanocrystalline iron produced by ball milling. *Scripta Metallurgica et Materialia*, 24, 1599-1604, ISSN: 0956-716X

Kalambur, W. & Hall, I. W. (1997). Dynamic compressive behavior of a SiC_w/Al composite. *Scripta Materialia*, 37, 2, 193-195, ISSN: 1359-6462

Kim, H. C.; Shon, I. J.; Yoon, J. K. & Doh, J. M. (2007). Consolidation of ultra fine WC and WC-Co hard materials by pulsed current activated sintering and its mechanical properties. *International Journal of Refractory Metals & Hard Materials*, 25, 46-52, ISSN: 0263-4368

Koch, C. C.; Cavin, C. G.; MacKaamey, C. G. & Scarbourgh, J. O. (1983). Preparation of "amorphous" $Ni_{60}Nb_{40}$ by mechanical alloying. *Applied Physics Letters*, 43, 1017-1019, ISSN: 0003-6951

Koch, C. C. (1993). The synthesis and structure of nanocrystalline materials produced by mechanical attrition: A Review. *Nanostructured Materials*, 2, 109-129, ISSN: 0965-9773

Lai, M. O. & Lu, L. (1998). *Mechanical alloying*. Kluwer Academic Publishers, ISBN: 978-0792380665, Norwell

Legendre, F.; Poissonnet, S. & Bonnallie, P. (2007). Synthesis of nanostructured SnO_2 materials by reactive ball-milling. *Journal of Alloys and Compounds*, 434, 400-404, ISSN: 0925-8388

Lu, L.; Lai, M. O. & Zhang, S. (1997) Diffusion in mechanical alloying. *Journal of Materials Processing Technology*, 67, 100-104, ISSN: 0924-0136

Lu, L. & Zhang, Y. F. (1999). Influence of process control agent on interdiffusion between Al and Mg during mechanical alloying. *Journal of Alloys and Compounds*, 290, 279-283, ISSN: 0925-8388

Ma, J.; Zhu, S. G.; Wu, C. X. & Zhang, M. L. (2009). Application of back-propagation neural network technique to high-energy planetary ball milling process for synthesizing nanocomposite WC-MgO powders. *Materials & Design*, 30, 2867-2874, ISSN: 0261-3069

Magini, M. & Iasonna, A. (1995). Energy-transfer in mechancial alloying. *Materials Transactions JIM*, 36, 133-123, ISSN: 0916-1821

Magini, M.; Iasonna, A. & Padella, F. (1996). Ball milling: An experimental support to the energy transfer evaluated by the collision model. *Scripta Materialia*, 34, 13-19, ISSN: 1359-6462

Munir, Z. A. (1988). Synthesis of high-temperature materials by self-propagating combustion methods. *American Ceramic Society Bulletin*, 67, 342-349, ISSN: 0002-7812

Murty, B. S.; Rao, M. M. & Ranganathan, S. (1995). Milling maps and amoprhization during mechanical alloying. *Acta Metallurgica et Materialia*, 43, 2443-2450, ISSN: 0956-7151

Razavi, M.; Rahimipour, M. R. & Mansoori, R. (2008). Synthesis of TiC nanocomposite powder from impure TiO_2 and carbon black by mechanically activated sintering. *Journal of Alloys and Compounds*, 450, 463-467, ISSN: 0925-8388

Richter, V. & Von Ruthendorf, M. (1999). On hardness and toughness of ultrafine and nanocrystalline hard materials. *International Journal of Refractory Metals & Hard Materials*, 17, 141-152, ISSN: 0263-4368

Rojac, T.; Kosec, A.; Malic, B. & Holc, J. (2006). The application of a milling map in the mechanochemical synthesis of ceramic oxides. *Journal of the European Ceramic Society*, 26, 3711-3716, ISSN: 0955-2219

Schaffer, G. B. & McCormick, P. G. (1990). Displacement reactions during mechanical alloying. *Metallurgical and Materials Transactions A*, 21, 2789-2794, ISSN: 1073-5623

Schwarz, R. B. & Koch, C. C. (1986). Formation of amorphous alloys by the mechanical alloying of crystalline powders of pure metals and powders of intermetallics. *Applied Physical Letters*, 49, 146-149, ISSN: 0003-6951

Sha, W. & Edwards, K. L. (2007). The use of artificial neural networks in materials science based research. *Materials & Design*, 28, 1747-1752, ISSN: 0261-3069

Sherif El-Eskandarany, M. (1996). Thermally assisted and mechanically driven solid-state reactions for formation of amorphous $AI_{33}Ta_{67}$ alloy powders. *Metallurgical and Materials Transactions A*, 27, 3267-3278, ISSN: 1073-5623

Sherif El-Eskandarany, M.; Aoki K.; Sumiyama K. & Suzuki K. (1997). Cyclic crystalline-amorphous transformations of mechanically alloyed $Co_{75}Ti_{25}$. *Applied Physics Letters*, 70, 1679-1681, ISSN: 0003-6951

Shetty, D. K.; Writght, I. G.; Mincer, P. N. & Clauer, A. H. (1985). Indentaion fracture of WC-Co cermets. *Journal of Materials Science*, 20, 1873-1882, ISSN: 0022-2461

Suryanarayana, C. & Sundaresan, R. (1991). Metastable phases in mechanically alloyed aluminum-manganese powder mixtures. *Materials Science and Engineering A*, 131, 237-242, ISSN: 0921-5093

Suryanarayana, C. (1995). Nanocrystalline materials. *International Materials Reviews*, 40, 41-64, ISSN: 0950-6608

Suryanarayana, C. & Koch, C. C. (1999). *Non-equilibrium Processing of Materials*. Pergamon, ISBN: 978-0080426976, Oxford

Suryananrayana, C. (2001). Mechanical alloying and milling. *Progress in Materials Science*, 46, 1-184, ISSN: 0079-6425

Suryanarayana, C. (2004). *Mechanical alloying and milling*. Marcel Dekker, ISBN:978-0824741037, New York

Takacs, L. (2002). Self-sustaining reactions induced by ball milling. *Progress in Materials Science*, 47, 355-414, ISSN: 0079-6425

Wang, K. Y.; Shen, T. D.; Wang, J. T. & Quan, M. X. (1991). Amorphization reaction during mechanical alloying: influence of the milling atmospheres. *Scripta Metallurgica et Materialia*, 25, (1991), 2227-2231, ISSN: 0956-716X

Watanabe, R.; Hashimoto, H. & Park, Y. H. (1991). Production of amorphous powder of Ti-Al intermetallic compound by vibratory ball milling. In: *Advances in powder metallurgy*, Pease III, L. F. & Sansoucy, R. J., (Ed.), 19-30, Metal Powder Industries Federation, ISBN: 978-1878954084, Princeton

Wright, L. G. & Wilcox, A. (1974). Observations on strengthening and oxidation behavior of a dispersion hardened Fe-Cr-Base alloy prepared by mechanical alloying. *Metallurgical and Materials Transactions*, 5, 957-960, ISSN: 1073-5615

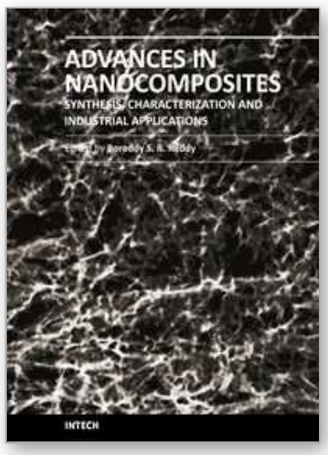
Wu, C. X.; Zhu, S. G.; Ma, J.; Zhang, M. L. (2009). Synthesis and formation mechanisms of nanocomposite WC-MgO powders by high-energy reactive milling. *Journal of Alloys and Compounds*, 478, 615-619, ISSN: 0925-8388

Wu, C. X.; Zhu, S. G.; Luo, Y. L. (2010).Effects of stearic acid on synthesis of nanocomposite WC-MgO powders by mechanical alloying. *Journal of Materials Science*, 45, 1817-1822, ISSN: 0022-2461

Yang, J. Y.; Zhang, T. J.; Cui, K. & Zhang, Z. H. (1997). Analysis of impact behavior during ball milling. *Acta Metallirgica Sinica*, 33, 381-385, ISSN: 0412-1961

Zhang, J. S.; Sun, Z. Q.; Chen, G. L.; Liu, X. J.; Cui, H. & Duan, X. J. (1997). Microstructure and properties of spray-deposited 2014+15 vol pct SiC particulate-reinforced metal matrix composite. *Metallurgical and Materials Transactions A*, 28, 5, 1261-1269, ISSN:1073-5623

Zhang, M.L.; Zhu, S. G.; Ma, J.; Wu, C. X.; Synthesis of nanosized WC/MgO powders by high energy ball milling and analysis of reaction thermodynamics. *Powder Metallurgy*, 53, 169-173, ISSN: 0032-5899



Advances in Nanocomposites - Synthesis, Characterization and Industrial Applications

Edited by Dr. Boreddy Reddy

ISBN 978-953-307-165-7
Hard cover, 966 pages
Publisher InTech
Published online 19, April, 2011
Published in print edition April, 2011

Advances in Nanocomposites - Synthesis, Characterization and Industrial Applications was conceived as a comprehensive reference volume on various aspects of functional nanocomposites for engineering technologies. The term functional nanocomposites signifies a wide area of polymer/material science and engineering, involving the design, synthesis and study of nanocomposites of increasing structural sophistication and complexity useful for a wide range of chemical, physicochemical and biological/biomedical processes. "Emerging technologies" are also broadly understood to include new technological developments, beginning at the forefront of conventional industrial practices and extending into anticipated and speculative industries of the future. The scope of the present book on nanocomposites and applications extends far beyond emerging technologies. This book presents 40 chapters organized in four parts systematically providing a wealth of new ideas in design, synthesis and study of sophisticated nanocomposite structures.

How to reference

In order to correctly reference this scholarly work, feel free to copy and paste the following:

Shigen Zhu, Jun Ma, Meilin Zhang and Caixia Wu (2011). Mechanical Alloying: For Formation of Nanocomposite WC/MgO Materials, Advances in Nanocomposites - Synthesis, Characterization and Industrial Applications, Dr. Boreddy Reddy (Ed.), ISBN: 978-953-307-165-7, InTech, Available from: http://www.intechopen.com/books/advances-in-nanocomposites-synthesis-characterization-and-industrial-applications/mechanical-alloying-for-formation-of-nanocomposite-wc-mgo-materials

INTECH
open science | open minds

InTech Europe
University Campus STeP Ri
Slavka Krautzeka 83/A
51000 Rijeka, Croatia
Phone: +385 (51) 770 447
Fax: +385 (51) 686 166
www.intechopen.com

InTech China
Unit 405, Office Block, Hotel Equatorial Shanghai
No.65, Yan An Road (West), Shanghai, 200040, China
中国上海市延安西路65号上海国际贵都大饭店办公楼405单元
Phone: +86-21-62489820
Fax: +86-21-62489821

© 2011 The Author(s). Licensee IntechOpen. This chapter is distributed under the terms of the Creative Commons Attribution-NonCommercial-ShareAlike-3.0 License, which permits use, distribution and reproduction for non-commercial purposes, provided the original is properly cited and derivative works building on this content are distributed under the same license.

IntechOpen

IntechOpen